Deep tissue multiphoton microscopy using longer wavelength excitation

Demirhan Kobat[1,*], Michael E. Durst[1], Nozomi Nishimura[2], Angela W. Wong[2], Chris B. Schaffer[2], and Chris Xu[1]

[1]*School of Applied and Engineering Physics, Cornell University, Ithaca, NY, 14853, USA*
[2]*Department of Biomedical Engineering, Cornell University, Ithaca, NY, 14853, USA*
[*] *dk287@cornell.edu*

Abstract: We compare the maximal two-photon fluorescence microscopy (TPM) imaging depth achieved with 775-nm excitation to that achieved with 1280-nm excitation through *in vivo* and *ex vivo* TPM of fluorescently-labeled blood vessels in mouse brain. We achieved high contrast imaging of blood vessels at approximately twice the depth with 1280-nm excitation as with 775-nm excitation. An imaging depth of 1 mm can be achieved in *in vivo* imaging of adult mouse brains at 1280 nm with approximately 1-nJ pulse energy at the sample surface. Blood flow speed measurements at a depth of 900 μm are performed.

OCIS codes:(170.3880) Medical and biological imaging, (180.4315) Nonlinear microscopy.

References and links

1. D. Kleinfeld, P.P. Mitra, F. Helmchen, and W. Denk, "Fluctuations and stimulus-induced changes in blood flow observed in individual capillaries in layers 2 through 4 of rat neocortex," Proc. Natl. Acad. Sci. USA **95**, 15741-15746 (1998).
2. K. Svoboda, F. Helmchen, W. Denk, and D. W. Tank, "Spread of dendritic excitation in layer 2/3 pyramidal neurons in rat barrel cortex in vivo," Nat. Neuroscience **2**, 65-73 (1999).
3. F. Helmchen, K. Svoboda, W. Denk, and D. W. Tank, "In-vivo dendritic calcium dynamics in deep-layer cortical pyramidal neurons," Nat. Neuroscience **2**, 989-996 (1999).
4. F. Helmchen, and W. Denk, "Deep tissue two-photon microscopy," Nat. Methods **2**, 932-940 (2005).
5. P. Theer, M.T. Hasan, and W. Denk, "Two-photon imaging to a depth of 1000 μm in living brains by use of a Ti:Al_2O_3 regenerative amplifier," Opt. Lett. **28**, 1022-1024 (2003).
6. M. Müller, J. Squier, R. Wolleschensky, U. Simon, and G. Brakenhoff, "Dispersion pre-compensation of 15 femtosecond optical pulses for high-numerical-aperture objectives," J. Microsc. **191**, 141-150 (1998).
7. S. Sakadzić, U. Demirbas, T.R. Mempel, A. Moore, S. Ruvinskaya, D.A. Boas, A. Sennaroglu, F.X. Kaertner, and J.G. Fujimoto, "Multi-photon microscopy with a low-cost and highly efficient Cr:licaf laser," Opt. Express **16**, 20848-20863 (2008).
8. P. Theer, and W. Denk, "On the fundamental imaging-depth limit in two-photon microscopy," J. Opt. Soc. Am. A **23**, 3139-3149 (2006).
9. A.N. Yaroslavsky, P.C. Schulze, I.V. Yaroslavsky, R. Schober, F. Ulrich, and H. Schwarzmaier, "Optical properties of selected native and coagulated human brain tissues in vitro in the visible and near infrared spectral range," Phys. Med. Biol. **47**, 2059-2073 (2002).
10. W. Cheong, S. Prahl, and A. Welch, "A review of the optical properties of biological tissues," IEEE J. Quantum Electron. **26**, 2166-2185 (1990).
11. I. Chen, S. Chu, C. Sun, P. Cheng, and B. Lin, "Wavelength dependent damage in biological multi-photon confocal microscopy: a micro-spectroscopic comparison between femtosecond Ti:sapphire and Cr:forsterite laser sources," Opt. Quantum Electron. **34**, 1251-1266 (2002).
12. J.M. Schmitt, A. Knuttel, M. Yadlowsky, and M.A. Eckhaus, "Optical-coherence tomography of a dense tissue: statistics of attenuation and backscattering," Phys. Med. Biol. **39**, 1705-1720 (1994).
13. B.E. Bouma, G.J. Tearney, I.P. Bilinsky, B. Golubovic, and J.G. Fujimoto, "Self-phase-modulated kerr-lens mode-locked Cr:forsterite laser source for optical coherence tomography," Opt. Lett. **21**, 1839-1841 (1996).
14. S. Chu, I. Chen, T. Liu, P.C. Chen, C. Sun, and B. Lin, "Multimodal nonlinear spectral microscopy based on a femtosecond Cr:forsterite laser," Opt. Lett. **26**, 1909-1911 (2001).

#111819 - $15.00 USD Received 26 May 2009; revised 2 Jul 2009; accepted 6 Jul 2009; published 20 Jul 2009

15. S. Chu, S. Chen, T. Tsai, T. Liu, C. Lin, H. Tsai, and C. Sun, "In vivo developmental biology study using noninvasive multi-harmonic generation microscopy," Opt. Express **11**, 3093-3099 (2003).
16. T. Tsai, C. Lin, H. Tsai, S. Chen, S. Tai, K. Lin, and C. Sun, "Biomolecular imaging based on far-red fluorescent protein with a high two-photon excitation action cross section," Opt. Lett. **31**, 930-932 (2006).
17. M. Balu, T. Baldacchini, J. Carter, T.B. Krasieva, R. Zadoyan, and B.J. Tromberg, "Effect of excitation wavelength on penetration depth in nonlinear optical microscopy of turbid media," J. Biomed. Opt. **14**, 010508-3 (2009).
18. T. Yasui, Y. Takahashi, M. Ito, S. Fukushima, and T. Araki, "Ex vivo and in vivo second-harmonic-generation imaging of dermal collagen fiber in skin: comparison of imaging characteristics between mode-locked Cr:forsterite and Ti:sapphire lasers," Appl. Opt. **48**, D88-D95 (2009).
19. L. Kou, D. Labrie, and P. Chylek, "Refractive indices of water and ice in the 0.65- to 2.5-μm spectral range," Appl. Opt. **32**, 3531-3540 (1993).
20. Q. Nguyen, P.S. Tsai, and D. Kleinfeld, "Mpscope: a versatile software suite for multiphoton microscopy," J. Neurosci. Methods **156**, 351-359 (2006).
21. A.Y. Shih, B. Friedman, P.J. Drew, P.S. Tsai, P.D. Lyden, and D. Kleinfeld, "Active dilation of penetrating arterioles restores red blood cell flux to penumbral neocortex after focal stroke," J. Cereb. Blood. Flow. Metab. **29**, 738-751 (2009).
22. D. Kleinfeld, and W. Denk, "Two-photon imaging of neocortical microcirculation," in *Imaging Neurons: A Laboratory Manual*, R. Yuste, F. Lanni, A. Konnerth, eds. (Cold Spring Harbor Laboratory Press, Cold Spring Harbor,2000) 23.1-23.15.
23. C.B. Schaffer, B. Friedman, N. Nishimura, L.F. Schroeder, P.S. Tsai, F.F. Ebner, P.D. Lyden, and D. Kleinfeld, "Two-photon imaging of cortical surface microvessels reveals a robust redistribution in blood flow after vascular occlusion," PLoS Biology **4**, e22 EP - (2006).
24. M. Friebel, J. Helfmann, U. Netz, and M. Meinke, "Influence of oxygen saturation on the optical scattering properties of human red blood cells in the spectral range 250 to 2000 nm," J. Biomed. Opt. **14**, 034001-6 (2009).
25. W.R. Zipfel, R.M. Williams, R. Christie, A.Y. Nikitin, B.T. Hyman, and W.W. Webb, "Live tissue intrinsic emission microscopy using multiphoton-excited native fluorescence and second harmonic generation," Proc. Natl. Acad. Sci. USA **100**, 7075-7080 (2003).
26. C. Xu, and W.W. Webb, "Measurement of two-photon excitation cross sections of molecular fluorophores with data from 690 to 1050 nm," J. Opt. Soc. Am. B **13**, 481-491 (1996).
27. Y. Liu, D.K. Cheng, G.J. Sonek, M.W. Berns, C.F. Chapman, and B.J. Tromberg, "Evidence for localized cell heating induced by infrared optical tweezers.," Biophys J. **68**, 2137–2144 (1995).
28. A. Schonle, and S.W. Hell, "Heating by absorption in the focus of an objective lens," Opt. Lett. **23**, 325-327 (1998).
29. W. Denk, D.W. Piston, and W.W. Webb, "Multi-photon molecular excitation in laser-scanning microscopy," in *Handbook of Biological Confocal Microscopy,* 3.ed., J.B. Pawlay, ed. (Springer Science, New York, NY, 2006) 535-549.
30. M. Müller, J. Squier, K.R. Wilson, and G.J. Brakenhoff, "3d microscopy of transparent objects using third-harmonic generation," J. Microsc. **191**, 266-274 (1998).
31. J.H. Lee, J. van Howe, C. Xu, S. Ramachandran, S. Ghalmi, and M.F. Yan, "Generation of femtosecond pulses at 1350 nm by Cerenkov radiation in higher-order-mode fiber," Opt. Lett. **32**, 1053-1055 (2007).
32. J. van Howe, J.H. Lee, S. Zhou, F. Wise, C. Xu, S. Ramachandran, S. Ghalmi, and M.F. Yan, "Demonstration of soliton self-frequency shift below 1300 nm in higher-order mode, solid silica-based fiber," Opt. Lett. **32**, 340-342 (2007).
33. A. Chong, W.H. Renninger, and F.W. Wise, "All-normal-dispersion femtosecond fiber laser with pulse energy above 20 nJ," Opt. Lett. **32**, 2408-2410 (2007).

1. Introduction

The three-dimensionally confined excitation volume of two-photon fluorescence microscopy (TPM) provides high-resolution images from deep within turbid biological samples. TPM has been used as a standard tool for the study of blood flow, neuronal activity, and anatomy in the cortex of rodent brain [1-3]. Imaging up to a depth of 600 μm for vasculature and 700 μm for neurons has been achieved with femtosecond modelocked Titanium:Sapphire (Ti:S) oscillators [4]. The maximum imaging depth in TPM depends on the ability of excitation light to reach the focus unscattered (ballistic excitation photons) and of emitted fluorescence to reach the detector. The maximum imaging depth scales linearly with the attenuation coefficient of the excitation light in tissue and logarithmically with average power incident on the sample surface, the duty cycle, and the collection efficiency. Theer *et al.* achieved 1 mm

#111819 - $15.00 USD Received 26 May 2009; revised 2 Jul 2009; accepted 6 Jul 2009; published 20 Jul 2009

imaging depth using a Ti:S regenerative amplifier (~200 nJ) at a repetition rate of 200 kHz [5]. In addition to the cost and complexity of an amplified laser system, the reduced repetition rate of the excitation source (from a typical 100 MHz to 200 kHz) limits the imaging speed and requires precise synchronization of excitation pulses with image acquisition. Reduction of the pulse width leads to increased two-photon fluorescence excitation but requires careful dispersion management in the microscope [6]. Furthermore, as the duration of the laser pulse is decreased, the width of the laser spectrum can approach and exceed the width of the two-photon excitation spectrum of the dye, limiting the benefit of shorter pulses [7]. Ultimately, the out-of-focus fluorescence generated near the surface limits the imaging depth [8]. Such an out-of-focus background cannot be mitigated by increasing the two-photon excitation efficiency.

A more effective strategy for improving the imaging depth is reduction of the attenuation of excitation light by tissue. As a result of the large difference between scattering mean free paths (MFPs) and absorption lengths in brain tissue [9,10], scattering dominates over absorption by water and intrinsic molecules in determining the attenuation factor for wavelengths between 350 nm and 1300 nm. We propose using longer excitation wavelengths, specifically the 1300-nm region, in order to reduce the effect of scattering. The use of longer excitation wavelengths will typically result in longer wavelength fluorescence emissions, where there is less absorption due to intrinsic tissue molecules [9], yielding an additional increase in imaging depth due to an increase in signal collection. We note that the use of longer excitation wavelengths will yield lower resolution images since the diffraction limited spot size scales linearly with wavelength in each dimension. However, considering the great benefits in depth penetration, the slight loss of resolution is a reasonable comprise. An additional advantage of the longer excitation wavelength over the conventional two-photon excitation window is its diminished phototoxicity. It has been experimentally shown that the 1300-nm excitation is much less phototoxic than the 800-nm excitation [11]. The superior penetration depth of 1300-nm excitation over 800-nm excitation has been demonstrated [12] and 1300-nm light sources has been used extensively for optical coherence tomography imaging [13].

There have been previous studies utilizing the penetration depth advantage of longer wavelength excitation, particularly Cr:Forsterite lasers. Multimodal imaging at 1230-nm excitation wavelength was demonstrated by imaging plant cell walls with second harmonic generation (SHG), third harmonic generation (THG), and endogenous two-photon fluorescence [14], zebrafish embryos with multi-harmonic generation [15] and with the two-photon fluorescence of far-red fluorescent protein [16]. Recent reports showed improved imaging depth using 1300-nm excitation compared to 800-nm excitation due to reduced scattering in tissue phantoms and in organotypic tissue models for two-photon fluorescence microscopy [17] and in *in vivo* and *ex vivo* skin tissue for second harmonic generation microscopy [18]. In this study, we compare the maximal TPM imaging depth achieved with 775-nm excitation to that achieved with 1280-nm excitation using *in vivo* and *ex vivo* TPM of fluorescently-labeled vasculature in the cortex of mouse brain. Approximately 1-mm imaging depth can be achieved in *in vivo* imaging of an adult mouse brain at 1280 nm. We record blood flow speed in individual cortical vessels at depths of up to 900 μm. Sample heating due to water absorption at this longer wavelength window will also be discussed.

2. Setup

Two femtosecond excitation sources, a Ti:S oscillator (λ_{center}=775 nm, Tsunami, Spectra Physics, Inc.) and a Ti:S-pumped optical parametric oscillator (OPO, λ_{center}=1280 nm, OpalBB, Spectra Physics, Inc.), are used for imaging. We chose 1280 nm as the longer excitation wavelength since it is close to a local minimum in the absorption spectrum of water (Fig. 1(c)) and to a peak in the two-photon excitation spectrum of a bright fluorophore

#111819 - $15.00 USD Received 26 May 2009; revised 2 Jul 2009; accepted 6 Jul 2009; published 20 Jul 2009

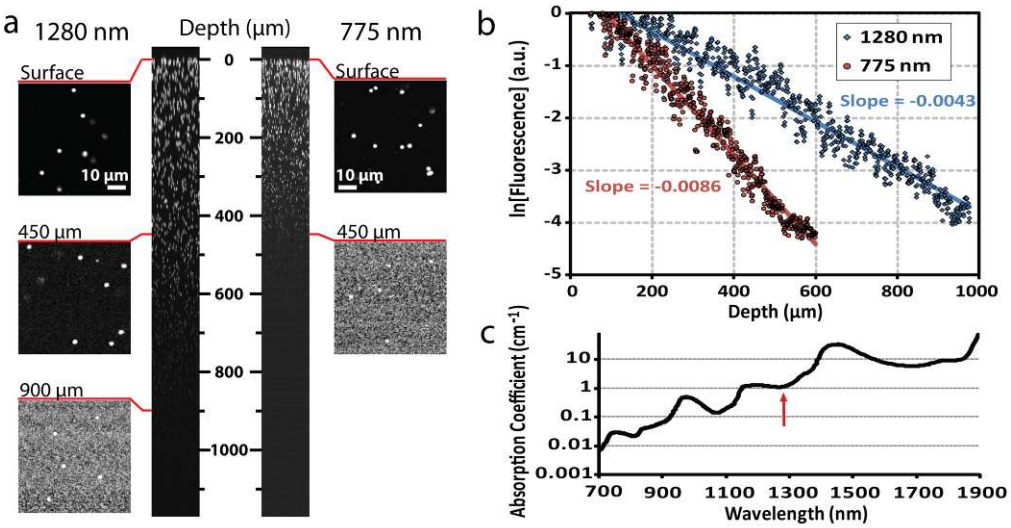

Fig. 1. TPM of fluorescent beads in a tissue phantom. (a) Maximum-intensity side projections of the image stacks for 1280-nm excitation and 775-nm excitation are shown on the left and right, respectively. Normalized single planar TPM images from several different depths are shown on each side. Each stack consists of 1200 x-y images (512x512 pixels, averaged over four scans, 4 fps) taken at a depth increment of 1 μm. (b) Fluorescence signal from single beads versus imaging depth. Points denote the average value of the brightest 0.1% of the pixels in a single x-y image on a logarithmic scale, and solid lines are exponential fits. (c) Absorption spectrum of water from 700 nm to 1900 nm [19].

(Alexa680) (Fig. 7). The repetition rate for both lasers is 82 MHz, and the pulse widths are approximately 100 fs and 140 fs for the Ti:S laser and OPO, respectively. The power of each beam is controlled by a half-wave plate and a polarization beam splitter cube. The raster-scanned beam is focused into the sample by a high numerical aperture water immersion microscope objective (Olympus XLUMPlanFl 20x 0.95NA). Due to the size the scan mirrors (3-mm aperture) and the expansion ratio (4X) in our microscope the laser beam fills about 60% of the back aperture of the objective lens (20 mm), resulting in an effective excitation numerical aperture about 0.6. We measured the transmission of the objective lens as 62% and 57% at 775 nm and 1280 nm, respectively. The fluorescence from the sample is epi-collected and directed to a photomultiplier tube (PMT) by a dichroic mirror. We use a bi-alkali PMT (H5783, Hamamatsu) for 775-nm excited TPM and a multi-alkali PMT (H5783-01, Hamamatsu) for 1280-nm excited TPM. The objective is translated axially within a movable objective microscope head (MOM, Sutter Instrument Company). Translation of the objective and image acquisition is controlled by a computer running MPScope [20]. Image processing and analysis are performed by ImageJ and MATLAB (Mathworks) software. A median filter with 1 pixel radius is applied to all image stacks in this work.

3. Experiments and results

The effects of scattering and water absorption on imaging depth with longer excitation wavelength can be demonstrated in tissue phantoms. We prepared a mixture of 1-μm diameter fluorescent beads as contrast agents and 1-μm diameter non-fluorescent beads (Polysciences Inc.) as scattering elements in a low-melting point agarose gel (Sigma-Aldrich). Yellow/green (505/515) beads (Invitrogen) and red (660/690) beads (Bangs Labs) were mixed together to obtain images from both excitation wavelengths. In order to eliminate external factors in this imaging depth comparison, such as the difference in two-photon responses of yellow/green and red beads and the difference in sensitivity of bi-alkali and multi-alkali PMTs, the power

#111819 - $15.00 USD Received 26 May 2009; revised 2 Jul 2009; accepted 6 Jul 2009; published 20 Jul 2009

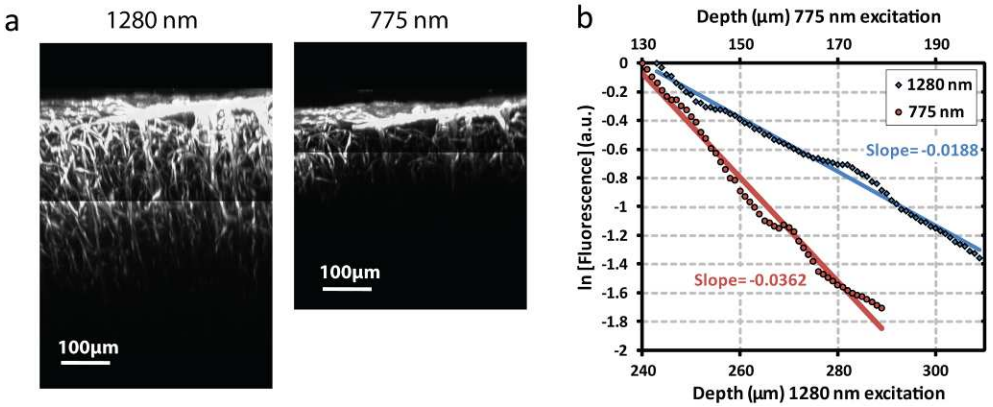

Fig. 2. *Ex vivo* TPM of cortical vasculature in a mouse brain. Blood vessels are filled with agarose gel that is stained by a mixture of fluorescein-dextran and Alexa680-dextran. (a) Maximum-intensity side projections of stacks for 1280-nm excitation (530 x-y images, 1-µm z increment) and for 775-nm excitation (330 x-y images, 1-µm z increment) are shown on the left and right, respectively. Each x-y image is 512x 512 pixels, averaged over four scans and taken at a 3-fps rate. (b) Attenuation of the measured fluorescence intensity with depth. Fluorescence signal strength at a particular depth is represented by the average value of the brightest 10% of the pixels in the x-y image from that depth.

of each excitation source was adjusted so that detected photon counts per bead were the same at the sample surface for both excitation wavelengths. A stack of x-y plane images was recorded at a depth increment of 1 µm starting from the surface at constant excitation power (Fig. 1). As the focus went deeper, the two-photon fluorescence signal with 775-nm excitation decayed approximately twice as fast as that with 1280-nm excitation. To quantitatively illustrate this result, we plotted the logarithm of the average value of the brightest 0.1% of the pixels from each frame as a function of depth for both excitation wavelengths (Fig. 1(b)). From the exponential fits to the data it is possible to determine a characteristic attenuation length (CAL), which corresponds to an e^{-2} fold decay in fluorescence signal. We obtained CAL values of 232 µm and 425 µm for 775-nm and 1280-nm excitation, respectively. Although the CAL takes into account the contributions from the excitation and the detection, the scattering of the excitation photons is the dominant attenuation mechanism in this sample, and the CAL should be close to the scattering MFP.

For *ex vivo* imaging, pentobarbital anesthetized mice (C57/BL6, 4 month-old) underwent cardiac perfusion with saline and 4% paraformaldehyde, immediately followed by perfusion with a low-melting point agarose gel that was labeled with a mixture of fluorescein-dextran and Alexa680-dextran (each 10-kD dextran, Invitrogen), each at a concentration of ~96 µM [21]. The brain was then extracted and post-fixed in 4% paraformaldehyde before imaging the fluorescently-labeled blood vessels in the cortex. All animal procedures were reviewed and approved by the Cornell Institutional Animal Care and Use Committee. To compare imaging at 775-nm and 1280-nm excitation, we adjusted the power of the excitation sources so that the same photon counts were produced from a brightly-labeled blood vessel at the sample surface. Power levels at sample surface were 60 mW for 775-nm excitation and 42 mW for 1280-nm excitation. We recorded a stack of x-y images at a depth increment of 1 µm. In order to avoid damaging the sample and photobleaching, relatively low power excitation was used for the shallow depths. The powers were increased once during the stack, keeping the ratio of the power of the two wavelengths constant. Figure 2(a) illustrates the x-z cross-section of the image stacks. We achieved high contrast imaging of labeled blood vessels at approximately twice the depth with 1280-nm excitation as with 775-nm excitation. In Fig. 2(b), the decay of fluorescence signal with imaging depth is shown. Fluorescence signal strength at a particular depth is represented by the average value of the brightest 10% of the pixels in the x-y image

#111819 - $15.00 USD Received 26 May 2009; revised 2 Jul 2009; accepted 6 Jul 2009; published 20 Jul 2009

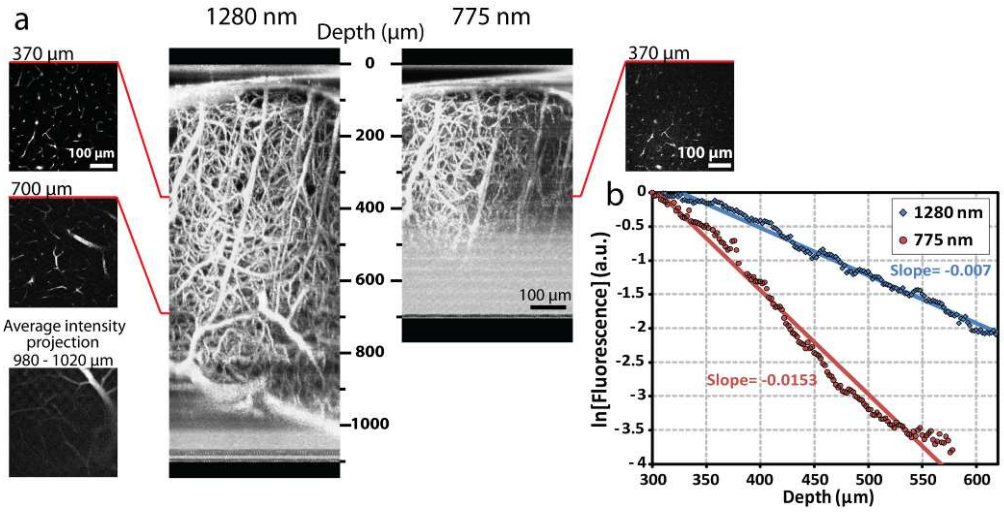

Fig. 3. *In vivo* TPM of cortical vasculature in a mouse brain. Blood plasma is labeled by FITC-dextran and Alexa680-dextran. (a) Maximum intensity side projections of normalized image stacks for 1280-nm excitation and for 775-nm excitation are shown on the left and right, respectively. Images are normalized by stretching the histogram to allow 0.5% of the pixels to be saturated. Normalized x-y images from several different depths are shown on each side. x-y images (512x512 pixels, averaged over three scans, 3 fps) in the stacks are taken at a depth increment of 2 μm. An average-intensity z projection of the x-y images at depths from 980 μm to 1020 μm is at the bottom left corner of the figure. (b) Attenuation of the measured fluorescence intensity with depth. Fluorescence signal strength at a particular depth is represented by the average value of the brightest 10% of the pixels in the x-y image from that depth.

from that depth. From the slopes of exponential fits to the data, we found that the CAL at 1280 nm is approximately twice that at 775 nm (106.4 μm and 55.2 μm, respectively), consistent with our observation of the imaging performance.

For *in vivo* imaging, mice (C57/BL6, 7 month-old, 20 g) were anesthetized using interperitoneally-injected urethane (150 mg / 100 g animal weight), and a craniotomy was performed above the parietal cortex. The dura was left intact. A glass coverslip was affixed to the skull using dental cement to seal the craniotomy. 200 μL of dye mixture (10 kDa FITC-dextran and 10 kDa Alexa680-dextran, each dissolved at 2.5% w/v in saline) was retro-orbitally injected to label the vasculature. Pulse oximetry was used to monitor heart rate and arterial oxygen saturation of the animal during surgery and imaging. Body temperature was maintained with a feedback-controlled heating blanket and rectal thermometer. The mouse was hydrated with 50 μL/hour subcutaneous injections of 5% glucose in saline. Imaging and power calibration (52 mW of 775 nm and 11.5 mW of 1280 nm at the sample surface) for *in vivo* imaging were done in the same way as the *ex vivo* TPM comparison. As shown in Fig. 3(a) and 3(b), observed differences between the imaging capabilities at depth of short and long wavelength excitation light were similar to the *ex vivo* comparison, with the maximum imaging depth at 1280 nm being approximately twice that at 775 nm. However, because *in vivo* brain tissue has longer scattering MFP than extracted and fixed tissue, much deeper imaging is possible with *in vivo* TPM. We measured the CAL to be 131 μm at 775 nm and 285 μm at 1280 nm. Kleinfeld and Denk measured a falloff constant for excitation intensities in the cortex of rat brain with a very similar methodology to that we use to determine the CAL. They found it to be roughly 200 μm for 830-nm excitation [22]. We achieved a 1-mm imaging depth with 1280-nm excitation using 93-mW (~ 1.1-nJ pulse energy) average power at the brain surface. Our imaging depth is comparable to that of the previous results using

#111819 - $15.00 USD Received 26 May 2009; revised 2 Jul 2009; accepted 6 Jul 2009; published 20 Jul 2009

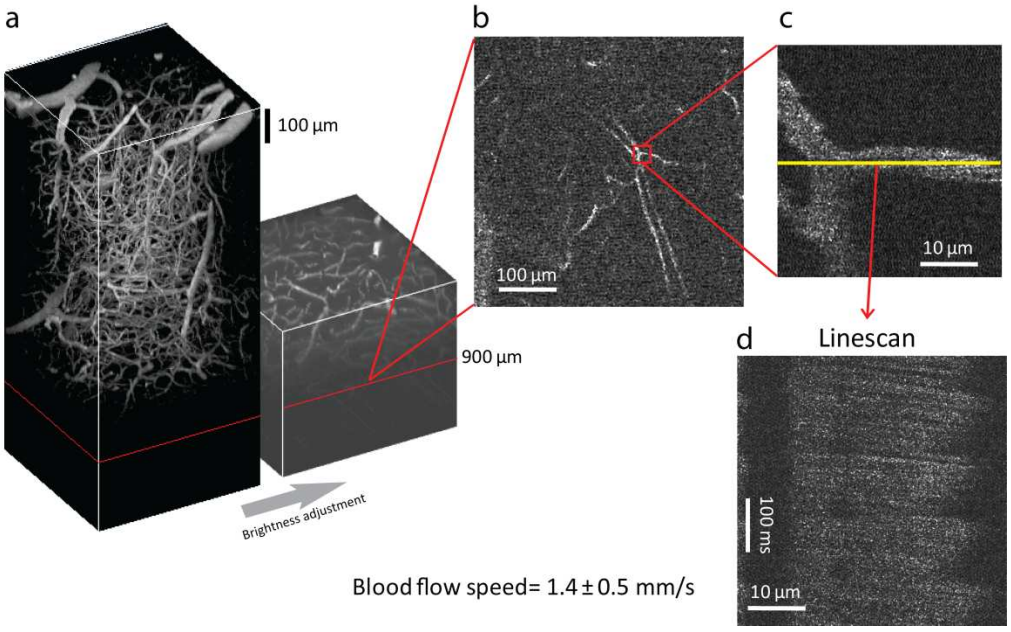

Fig. 4. Blood flow speed measurement in a single cortical capillary at a depth of 900 µm. (a) A 3-D rendering of the stacks was created using the volume viewer plug-in in ImageJ software. (b) A single normalized planar TPM image from a depth of 900 µm. (c) Zoomed in planar view of a capillary. We recorded line scans along the central axis of the vessel at a rate of ~1 ms per line. Line scan trajectory is marked by the yellow line. (d) x (spatial dimension) - t (temporal dimension) data set from the line scans. Dark bands are due to the motion of the unstained red blood cells (RBCs) along the scan direction. The slope of the bands gives the inverse of the speed of the RBCs [23]. We calculated the speed of RBCs in this deep capillary to be 1.4 mm/s with a standard deviation of 0.5 mm/s.

nearly 200-nJ excitation pulses at the sample surface at a wavelength of 925 nm [5]. Even at a 1-mm depth, capillary blood vessels can be clearly resolved, and the minimum spatial feature observed in our x-y image was approximately 3 µm. In this image stack, a clear transition in vascular morphology around 900-1000 µm indicates that the images span the entire depth of cortex. We note that our imaging depth is limited by the available excitation power, not by background from out-of-focus fluorescence excitation.

One major advantage of *in vivo* TPM is the capacity to image physiological dynamics. The improved penetration depth with 1280-nm excitation from an OPO enables imaging at a sufficiently high frame rate to resolve red blood cell motion in capillaries at the bottom of the cortex. We performed blood flow measurements in a cortical capillary at a depth of 900 µm using line scanning of the blood vessels (Fig. 4). The method for calculating the blood flow speed is described in Ref. [23]. The speed of the blood flow in the capillary shown in Fig. 4 was measured to be 1.4 mm/s with a standard deviation of 0.5 mm/s.

The longer wavelength excitation also provides advantages for *in vivo* imaging through blood vessels. Figure 5 shows the improved contrast for imaging fluorescently-labeled brain capillaries directly beneath a large blood vessel on the brain surface in a live mouse. We observed an approximately three to four times higher signal from the capillaries directly underneath a ~ 20-µm diameter vessel on the brain surface with 1280-nm excitation than with 775-nm excitation. There are three possible factors that together can result in this observation. The first is the difference in the scattering MFP at the two excitation wavelengths in blood. For example, in human blood (at a reduced hematocrit (Hct) of 33.2%) the scattering MFP is

#111819 - $15.00 USD Received 26 May 2009; revised 2 Jul 2009; accepted 6 Jul 2009; published 20 Jul 2009

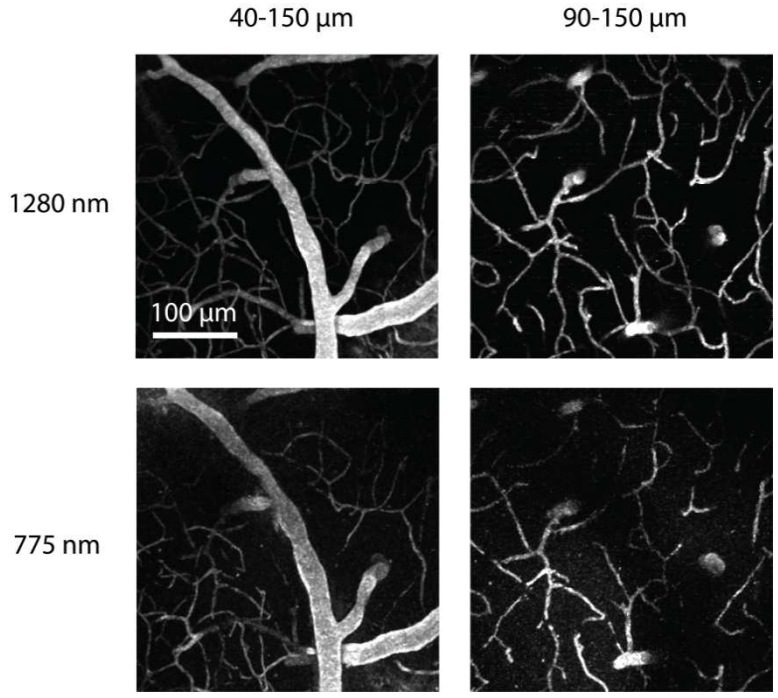

Fig. 5. Improved performance of *in vivo* two-photon imaging through blood vessels with longer wavelength excitation. Maximum intensity z-projections of TPM of the cortical vasculature with 1280-nm excitation (top row) and with 775-nm excitation (bottom row) are shown. The emission peak of Alexa680 (used with 1280-nm excitation) is at 700 nm, and the emission peak of FITC (used with 775-nm excitation) is at 518 nm. Left column is the projection of blood vessels between depths of 40 µm and 150 µm from the brain surface, showing relatively large blood vessels at the surface. Right column is the projection of the 60-µm slice beneath the large blood vessels. All images are normalized after the maximum intensity projections along the z-axis are performed. Reduction of the detected fluorescence intensity in the areas beneath the large blood vessels is significantly more pronounced with 775-nm excitation.

11.5 µm at 775 nm and 17.4 µm at 1280 nm [24]. The whole blood values (Hct 45%) would be virtually the same since scattering scales very weakly from Hct 33.2% to 45%. Going through 20 µm of blood would decrease the two-photon fluorescence generation by 90% and 97% for 1280-nm excitation and 775-nm excitation, respectively. However, by comparing the brightness of the vessels underneath large vessels to the brightness of the vessels that are not immediately underneath large vessels, we obtain approximately 40% and 85% attenuation for 1280-nm excitation and 775-nm excitation, respectively. This is possibly due to the contribution of non-ballistic photons to the two-photon excitation as scattering occurs very close to the focal plane. Nevertheless, the reduced scattering MFP at 1280 nm is still advantageous over 775 nm. The second factor is the absorption of the excited fluorescence signal by the blood, which is significantly reduced for ~700-nm emission range. We can again use human blood values for an estimation of the magnitude of this effect. In human blood (Hct 45%, linearly scaled from Hct 33.2% values in Ref. [24]) absorption length is ~74 µm at 515 nm (fluorescein emission) and ~3.7 mm at 700 nm (Alexa680 emission) [24]. This difference yields 1.3-fold less absorption of 700-nm photons with respect to 515-nm photons traveling through 20 µm of blood. The last possible factor is the wavefront distortion by the blood vessel due to the index of refraction mismatch, which leads to lower excitation intensities beneath the blood vessel. The amount of phase distortion in the wavefront inversely scales with the excitation wavelength. Therefore, 1280-nm excitation is affected less by this

#111819 - $15.00 USD Received 26 May 2009; revised 2 Jul 2009; accepted 6 Jul 2009; published 20 Jul 2009

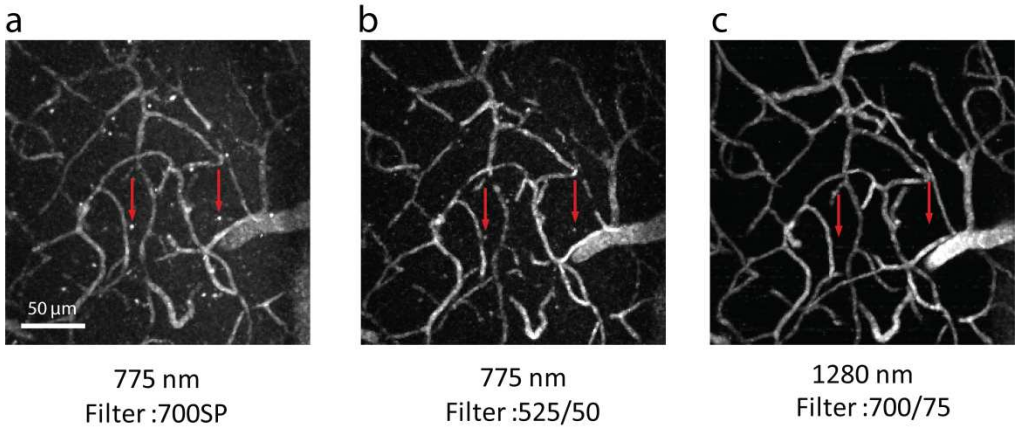

Fig. 6. Maximum intensity z-projections of *in vivo* TPM images of cortical vasculature between 80-µm and 180-µm depth using (a) 775-nm excitation and 700-nm short pass emission filter, (b) 775-nm excitation and 525-nm band-pass filter with 50-nm spectral bandwidth, and (c) 1280-nm excitation and 700-nm emission band-pass filter with 75-nm bandwidth. Red arrows indicate the positions of two exemplary intrinsically fluorescent structures. All three images are normalized after maximum intensity projections along z-axis are performed.

phenomenon compared to 775-nm excitation. Since almost all *in vivo* tissue has significant vasculature, the improved imaging capability through blood vessels provided by the longer wavelength excitation is highly valuable for *in vivo* imaging.

With 1200 to 1300-nm wavelength excitation light, intrinsic fluorescence from endogenous molecules such as NADH and flavin proteins will require three or more photon excitation and thus will be weakly excited compared to an extrinsic fluorophore that is two-photon excited in this wavelength range. In addition, the wavelength of intrinsic fluorescence [25] is significantly shorter than that of the long-wavelength extrinsic fluorophores used here, providing additional discrimination. This phenomenon is demonstrated in Fig. 6, where maximum intensity z projections in *in vivo* mouse brain are shown for three stacks of images of the same region using different optical filters and different excitation wavelengths. In the first stack (Fig. 6(a)), which was taken using 775-nm excitation with a 700-nm short-pass emission filter (ET700SP, Chroma), bright structures due to intrinsic fluorescence are clearly visible along with FITC-labeled blood vessels. Switching to a narrow band-pass filter (HQ525/50, Chroma) that centers on the FITC emission spectrum decreased the contribution from intrinsic fluorescence with respect to FITC fluorescence signal (Fig. 6(b)), but it was not possible to eliminate the auto-fluorescence signal completely. In the stack acquired with 1280-nm excitation and a ET700/75 (Chroma) emission filter (Fig. 6(c)), however, the intrinsic fluorescence signal is absent from the images. We conclude that the longer excitation wavelength should benefit imaging of extrinsic indicators with higher contrast through weaker excitation and more effective optical filtering of the intrinsic fluorescence background.

To establish the utility of longer wavelength TPM for biological imaging, we measured the two-photon excitation cross-sections of several commercially available fluorophores from 1220 nm to 1320 nm (Fig. 7) following the methodology described in Ref. [26]. The two-photon excitation maxima of two of these fluorophores (Alexa680 and Cy5.5) were within our measured wavelength range, and their two-photon action cross-sections (50-75 GM range)are comparable with those of widely used shorter wavelength excitable dyes, such as rhodamine B and fluorescein [26].

4. Discussions

Although the effect of absorption is negligible compared to scattering for the attenuation of ballistic excitation photons, it should be taken into consideration in terms of sample heating. It

#111819 - $15.00 USD Received 26 May 2009; revised 2 Jul 2009; accepted 6 Jul 2009; published 20 Jul 2009

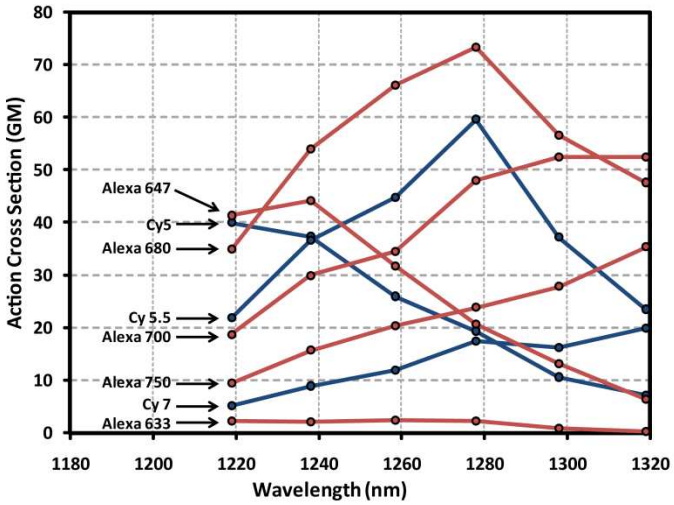

Fig. 7. Two-photon action cross-sections (quantum efficiency (η_2) x absolute two-photon cross-section (σ_2)) of 8 commercial dyes. Solid lines are guides for the eye.

was established, both experimentally and by numerical calculation, that the temperature increase at the focal point of a laser scanning microscope is negligible [27,28]. This follows from the rapid heat diffusion inside biological tissues and beam scanning. Although 93 mW of 1280-nm excitation power is used at the sample surface for imaging at a depth of 1-mm, the excitation power within the focal volume is significantly smaller due to the scattering of the sample. Following the work of Refs. [27] and [28], we estimate the temperature rise at the focal volume to be a small fraction of 1 K. For the heating in regions close to the sample surface, where the illumination is mostly stationary due to the reduced effect of beam scanning, an upper bound estimate can be calculated by the model described in Ref. [29], which is based on 2D heat diffusion in an infinite sample. We calculated the maximum temperature rise to be approximately 0.9 K and 4.2 K after 1 second and 1 minute of continuous illumination, respectively, for a uniform beam with a diameter of 1.4 mm (100 mW average power and 1280 nm excitation wavelength). While the model described in Ref. [29] is probably adequate for the short time-scale, the logarithmic divergence of the temperature increase as a function of time is likely a significant over-estimate for the long time-scale. Factors which are ignored by the passive 2D heat diffusion model such as axial heat diffusion, heat exchange with the surrounding environment (e.g. the cover slip and the immersion liquid), and heat transfer through blood circulation must be taken into account. By treating blood vessels as heat reservoirs with constant temperature, for example, a steady state solution to the temperature rise at the surface can be found by solving the 2D diffusion equation with the boundary condition of constant temperature. We found the temperature rise to be less than 1 K. Finally, we note that for the same excitation power at the focal plane, the power at the sample surface will be less for 1280-nm excitation than for 775-nm excitation due to the reduced power attenuation by scattering in tissue. Therefore beyond a certain imaging depth (approximately 3.7 scattering MFP at 1280 nm, using the fact that the CAL at 1280 nm is twice of the CAL at 775 nm), 1280-nm excitation results in less heat generation even though it is more strongly absorbed by water.

One of the major challenges of the longer wavelength imaging is the excitation source. A Ti:S pumped OPO was used in our experiment. There are other excitation sources such as optical parametric amplifiers and the Cr:Forsterite lasers that have been used in TPM [14,16] and multi-harmonic generation imaging [14,15,30]. However, these sources have much lower average power output when compared to the Ti:S laser. The extra cost and reliability issues

#111819 - $15.00 USD Received 26 May 2009; revised 2 Jul 2009; accepted 6 Jul 2009; published 20 Jul 2009

are also major disadvantages in using the OPO for TPM. A robust and energetic pulsed source is essential for the longer wavelength excitation region to be widely accessible for multiphoton microscopy (MPM). Several recent developments in fiber-based femtosecond lasers [31-33] are promising as the potential excitation sources for the longer wavelength MPM.

5. Conclusions

The excitation window at 1300 nm allows for deeper TPM in biological specimens than the conventional 700 to 1100-nm excitation window afforded by Ti:S laser systems. Both *in vivo* and *ex vivo* TPM of vasculature in mouse brain demonstrated that 1280-nm excitation performs approximately twice as well as 775-nm excitation in terms of imaging depth. An imaging depth of 1 mm was achieved in *in vivo* imaging of adult mouse brains at 1280 nm with approximately 1-nJ pulse energy at the sample surface. Using the superior depth penetration capability of 1280 nm we performed single capillary blood flow measurements at 900 μm. We observed an increased capability to image through blood vessels and a greater ability to suppress endogenous fluorescence background with 1280-nm excitation. We also presented the two-photon excitation cross section measurements of commercially available fluorophores that can be two-photon excited at ~ 1300 nm.

Acknowledgements

This research project is supported by NSF/DBI (Grant: DBI-0546227; C.X.) and the American Heart Association (Grant: 0735644T; C.B.S.). We thank Jinhao Ruan for his contributions in two-photon excitation cross section measurements and Warren R. Zipfel and Rebecca M. Williams for discussions and technical suggestions.

#111819 - $15.00 USD Received 26 May 2009; revised 2 Jul 2009; accepted 6 Jul 2009; published 20 Jul 2009